Current-induced out-of-plane torques in a single permalloy layer with lateral structural asymmetry

Motomi Aoki,[1] Ei Shigematsu,[1] Ryo Ohshima,[1] Teruya Shinjo,[1] Masashi Shiraishi,[1] and Yuichiro Ando[1,2,*]
[1]Department of Electronic Science and Engineering, Kyoto University, Kyoto 615-8510, Japan
[2]PRESTO, Japan Science and Technology Agency, Honcho, Kawaguchi, Saitama 332-0012, Japan

(Received 23 December 2021; revised 25 February 2022; accepted 23 March 2022; published 7 April 2022)

We investigated current-induced torques in a single permalloy layer connected to nonmagnetic electrodes with lateral inversion asymmetry by spin-torque ferromagnetic resonance. Considering the symmetry of the spin-torque ferromagnetic resonance spectrum with respect to the magnetic field direction, we successfully separated various types of torque. In addition to in-plane damping-like and field-like torques, we detected two additional components of out-of-plane (OOP) torques, the symmetries of which with respect to the magnetic field direction correspond to an OOP field-like torque and an OOP damping-like torque. We obtained the OOP torques in particular by breaking a lateral inversion symmetry of the nonmagnetic electrodes, and the sign of the torques is reversed by inverting the electrode structure. The microwave frequency dependence of the OOP torques indicates that the OOP torques are not attributable to a spin current but to the Oersted field generated by a nonuniform charge current, B_{Oersted}, and an inductive field, $B_{\mathrm{induc.}}$ (which originates from B_{Oersted}). We propose an external field-free and fast magnetization switching of a ferromagnetic layer with perpendicular magnetic anisotropy by using $B_{\mathrm{induc.}}$, which can be achieved only by fabricating the electrodes asymmetrically.

DOI: 10.1103/PhysRevB.105.144407

I. INTRODUCTION

Charge-to-spin (C-S) conversion is one of the most widely studied phenomena in spintronics research [1–6] because efficient C-S conversion will facilitate highly endurable magnetoresistive random access memory (MRAM) [7–11]. Breaking of spatial inversion symmetry is essential to C-S conversion. For example, when an electric current flows along the x direction, the broken inversion symmetry along the z direction generates a spin polarization along the y direction. A representative case is the Rashba-Edelstein effect (REE) [12], where C-S conversion occurs at an interface of the heterostructure. Such spin polarization can diffuse into an adjacent ferromagnetic material (FM) and impart torque to the magnetization [13,14]. Current-induced torques imparted by the spin polarization along the y direction are classified into two components: the in-plane (IP) field-like (FL) torque ($\sim \boldsymbol{y} \times \boldsymbol{M}$) and the IP damping-like (DL) torque [$\sim \boldsymbol{M} \times (\boldsymbol{M} \times \boldsymbol{y})$], where $\boldsymbol{M}$ is the vector of the magnetization [15,16]. The IP DL torque can be used for magnetization switching of a FM with IP magnetic anisotropy [8,17,18]. However, the IP DL torque cannot be used for a FM with perpendicular magnetic anisotropy (PMA) unless an additional external magnetic field is applied [7,19], although PMA is advantageous in terms of integrating MRAM.

Recently, as a counterpart of the REE, current-induced out-of-plane (OOP) torques via broken lateral inversion symmetry induced by a broken crystalline symmetry [20,21] or an artificial wedge structure [22] have been reported. OOP torques are classified into two components: the OOP FL torque ($\sim \boldsymbol{z} \times \boldsymbol{M}$) and the OOP DL torque [$\sim \boldsymbol{M} \times (\boldsymbol{M} \times \boldsymbol{z})$] [20]. Because the OOP DL torque can induce field-free magnetization switching of a FM with PMA [23,24], generation of the OOP DL torque is strongly desired. However, in contrast to the broken vertical inversion symmetry that is readily induced by fabricating a heterostructure, introduction of lateral inversion symmetry is technically difficult. Although the aforementioned methods generate OOP torques, broken crystalline symmetry is nonversatile. Application of the artificial wedge structure to practical MRAM is also difficult because the broken lateral inversion symmetry should be introduced within the device, the size of which is generally less than 100 nm × 100 nm. To develop a simple method to introduce broken lateral inversion symmetry in small devices only by using familiar materials, in this study we focus on the lateral inversion symmetry of nonmagnetic electrodes connected to FM. Because a finite asymmetry can be induced by the distribution of a charge current flow, such asymmetry might contribute to inducing the OOP torques. By measuring the angular dependence of the external magnetic field of spin-torque ferromagnetic resonance (ST-FMR) signals, we obtained additional two components of OOP torques, the symmetries of which with respect to the magnetic field direction corresponded to OOP DL and FL torques. Furthermore, a sign of the OOP torques was reversed when we inverted the lateral symmetry of the electrode. However, the frequency dependence of the ST-FMR signals indicated that the OOP DL torque was mainly due to an inductive magnetic field, $B_{\mathrm{induc.}}$, generated by the eddy current. Although generation of the OOP DL torque originating from a spin current is not pertinent, we propose an external field-free magnetization switching of PMA by using $B_{\mathrm{induc.}}$, which remained after the IP DL and FL torques were no longer evident.

*ando.yuichiro.5s@kyoto-u.ac.jp

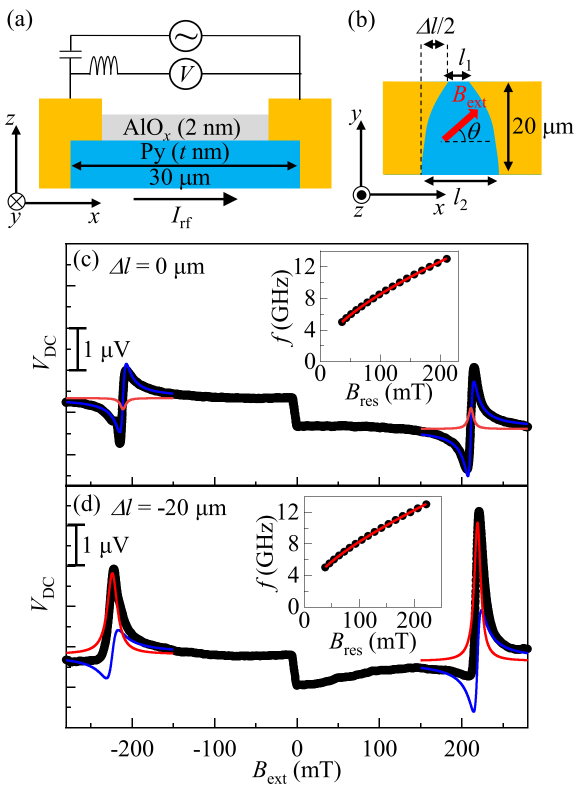

FIG. 1. (a) Schematics of device structure and electrical circuit. (b) View of the device structure from the z-axis. ST-FMR spectra when $f = 13$ GHz for (c) $\Delta l = 0$ μm and (d) -20 μm. Red and blue curves show the symmetric and antisymmetric Lorentzian components, respectively, obtained from the fitting of the ST-FMR spectrum. Insets show f as a function of B_{res}, and red curves are the fitting results by using the Kittel equation.

II. SAMPLE FABRICATION AND EXPERIMENTAL PROCEDURE

Figure 1(a) shows schematics of the device structure and the electrical circuit in this study. We used a single permalloy ($Ni_{81}Fe_{19}$, Py) layer to observe the OOP torques clearly, because in nonmagnetic material (NM)/FM bilayer structures, the torque via the Oersted field and the IP DL torque via the spin Hall effect (SHE) in NM are pertinent and hinder highly sensitive detection of OOP torques. A rectangular Py (5.5-nm)/Al (2-nm) layer was fabricated on a MgO (100) substrate using electron-beam lithography and electron-beam deposition. Deposition of the Al layer prevented oxidation of the Py layer. The electrical conduction of the Al (2-nm) layer was confirmed to be negligible after exposure to the air because of formation of the oxidation layer, AlO_x. Then, nonmagnetic Ti (3-nm)/Au (50-nm) electrodes with a coplanar waveguide structure were fabricated after Ar ion milling to obtain electrical contact. Figure 1(b) shows a schematic top view of the device structure from the By changing the shape of the Ti/Au electrodes, the lengths of the Py channel at each side (l_1 and l_2) were changed from 5 to 25 μm to break lateral inversion symmetry. Δl was changed from -20 μm to 20 μm, where $\Delta l = l_2$–l_1. ST-FMR was used to observe the magnitude and direction of the current-induced torques [15,25,26]. Under irradiation of a microwave electric current from a microwave source with an external magnetic field, B_{ext}, along the θ direction, the current-induced torques produced an oscillation of the magnetization and resulting oscillating resistance via anisotropic magnetoresistance (AMR) around the ferromagnetic resonance condition. The oscillating resistance was rectified by the rf electric current, I_{rf}, and a nonzero direct-current (DC) voltage, V_{DC}, was generated, which was measured with a nanovoltmeter via a bias tee. Regarding a plot of V_{DC} as a function of B_{ext}, the spectrum consists of symmetric and antisymmetric Lorentzian functions. In a NM/FM bilayer structure, the spin-orbit torque (SOT) produces the symmetric Lorentzian function, and the Oersted field via the electric current flowing in the NM layer is the main contributor to the antisymmetric Lorentzian. In this case, the torque efficiency can be estimated by taking the ratio between two Lorentzian functions. In a single FM layer, however, the aforementioned analysis is unavailable because the Oersted field via the electric current flowing in the FM layer does not impart a torque to the magnetization of the FM layer, and other contributions such as the IP FL torque and OOP torques become non-negligible. Therefore, the shape of each Lorentzian function was directly analyzed as explained in a subsequent paragraph. The microwave power was fixed to 5 dBm and all measurements were carried out at room temperature. The value of θ was fixed to 45 ° unless otherwise indicated.

III. SYMMETRY OF ST-FMR SIGNALS WITH RESPECT TO MAGNETIC FIELD DIRECTION

Figure 1(c) and 1(d) show ST-FMR spectra with a microwave frequency, $f = 13$ GHz, and the insets show f as a function of the FMR field, B_{res}, when $\Delta l = 0$ and –20 μm, respectively. In both cases, signals were well fitted by the sum of the symmetric and the antisymmetric Lorentzian functions expressed as [25]

$$V_{DC} = A\frac{\Gamma(B_{ext} - B_{res})}{(B_{ext} - B_{res})^2 + \Gamma^2} + S\frac{\Gamma^2}{(B_{ext} - B_{res})^2 + \Gamma^2}, \quad (1)$$

where A is the amplitude of the antisymmetric Lorentzian, S is the amplitude of the symmetric Lorentzian, and Γ is the half width at half maximum. In addition, f-B_{res} plots were well-fitted by the Kittel formula [27], $f = (2\pi/\gamma)\sqrt{B_{res}(B_{res} + \mu_0 M_{eff})}$, where γ is the gyromagnetic ratio, μ_0 is the vacuum permeability, and M_{eff} is the effective magnetization [Fig. 1(c) and 1(d)]. Therefore, we confirmed uniform excitation of FMR despite the reduced geometrical symmetry in the devices. Here, we focused on the symmetry in A and S under magnetic-field reversal. When $\Delta l = 0$ μm, both A and S were approximately antisymmetric; i.e., the magnitudes were unchanged but the signs were opposite with respect to the magnetic field direction [Fig. 1(c)]. However, when $\Delta l = $ –20 μm, A and S were obviously asymmetric; i.e., the magnitudes differed with respect to the magnetic-field direction [Fig. 1(d)]. To verify the origin of this asymmetry, we measured the θ dependence of the ST-FMR spectra. Figure 2(a)-2(f) shows the θ dependences of A and S for devices with $\Delta l = 0$ μm [Fig. 2(a) and 2(b)], $\Delta l = 20$ μm

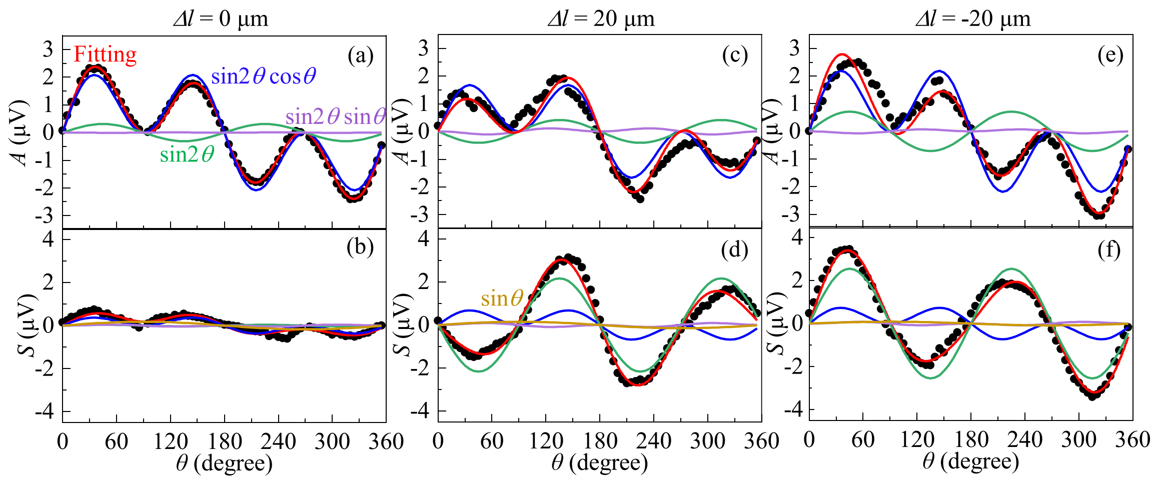

FIG. 2. θ dependence of (a) A and (b) S for a device with $\Delta l = 0$ μm. Those of devices with (c and d) $\Delta l = 20$ μm and (e and f) -20 μm are also shown. θ dependences of A are fitted by $\sin2\theta\cos\theta$ (blue), $\sin2\theta$ (green), and $\sin2\theta\sin\theta$ (purple). θ dependences of S are fitted by $\sin2\theta\cos\theta$ (blue), $\sin2\theta$ (green), $\sin2\theta\sin\theta$ (purple), and $\sin\theta$ (gold). Red curves are the sum of all of the components.

[Figs. 2(c) and 2(d)], and $\Delta l = -20$ μm [Figs. 2(e) and 2(f)]. In accordance with prior research, the θ dependence of A consists of three terms: $\sin2\theta\cos\theta$ (blue), $\sin2\theta\sin\theta$ (purple), and $\sin2\theta$ (green); and that of S consists of four terms: $\sin2\theta\cos\theta$ (blue), $\sin2\theta\sin\theta$ (purple), $\sin2\theta$ (green), and $\sin\theta$ (brown) [28,29] as shown in Tables S1 and S2 in Supplemental Material A [30]. The colors in brackets correspond to the color of the lines in Fig. 2. The origin of the $\sin2\theta$ dependence in all of the terms except for the $\sin\theta$ term in S is attributable to the differential of the AMR signals, and the other dependences are attributable to the θ dependence of the torque (Tables S1 and S2 in Supplemental Material A [30]). The contribution of the $\sin2\theta\sin\theta$ (purple) term originating from x-polarized spin [31] and that of the $\sin\theta$ (brown) term originating from spin pumping and the thermoelectric effect [32] were less than 6% of the sum of all the terms for all the devices, indicating that four types of torque are dominant: IP FL torque ($\sin2\theta\cos\theta$ in A), IP DL torque ($\sin2\theta\cos\theta$ in S), OOP FL torque ($\sin2\theta$ in S), and OOP DL torque ($\sin2\theta$ in A) [33], as summarized in Table I. In an ideal case, a net spin current along the z direction is expected to be zero because the adjacent materials of the top and bottom surfaces of the Py layer are both an insulator. However, when the anomalous SOT [34], nonuniform magnetism [35], stress coming from the substrate [36], or REE at the Py/AlO_x interface [13] are present, finite IP torques are expected. The asymmetry in the ST-FMR spectra with respect to the magnetic-field direction [Fig. 1(d)] originated from the difference in symmetry under 180° rotations between $\sin2\theta\cos\theta$ and $\sin2\theta$. Therefore, we can estimate the effective magnetic fields corresponding to each torque by addition and subtraction operations [26],

$$S_{\text{odd}} \equiv \frac{S_\theta - S_{180^\circ+\theta}}{2} = B_{\text{DL},y}\frac{\pi w t R_{\text{AMR}} f}{\Gamma\gamma(2B_{\text{res}} + \mu_0 M_{\text{eff}})}\sin2\theta\cos\theta, \quad (2a)$$

$$S_{\text{even}} \equiv \frac{S_\theta + S_{180^\circ+\theta}}{2} = -B_{\text{FL},z}\frac{\pi w t R_{\text{AMR}} f}{\Gamma\gamma(2B_{\text{res}} + \mu_0 M_{\text{eff}})}\sin2\theta, \quad (2b)$$

$$A_{\text{odd}} \equiv \frac{A_\theta - A_{180^\circ+\theta}}{2} = -B_{\text{FL},y}\frac{w t R_{\text{AMR}}(B_{\text{res}} + \mu_0 M_{\text{eff}})}{2\Gamma(2B_{\text{res}} + \mu_0 M_{\text{eff}})}\sin2\theta\cos\theta, \quad (2c)$$

and

$$A_{\text{even}} \equiv \frac{A_\theta + A_{180^\circ+\theta}}{2} = -B_{\text{DL},z}\frac{w t R_{\text{AMR}}(B_{\text{res}} + \mu_0 M_{\text{eff}})}{2\Gamma(2B_{\text{res}} + \mu_0 M_{\text{eff}})}\sin2\theta, \quad (2d)$$

where $B_{\text{DL},y(z)}$ and $B_{\text{FL},y(z)}$ represent the effective DL and FL field, respectively; w is the width of the channel; $\hbar$ is the Dirac constant; e is the elementary charge; M_s is the saturation magnetization; and t is the thickness of the Py layer. We used the fact that the AMR in our devices has the form $R = R_0 + R_{\text{AMR}}\sin^2\theta$ (Supplemental Material B [30]). The Oersted field along the y and z directions were included in $B_{\text{FL},y}$ and $B_{\text{FL},z}$, respectively. Here, directions of $B_{\text{DL},y}$, $B_{\text{FL},z}$, $B_{\text{FL},y}$, and $B_{\text{DL},z}$ are along $\boldsymbol{y}\times\boldsymbol{M}$, $\boldsymbol{z}$, $\boldsymbol{y}$, and $\boldsymbol{z}\times\boldsymbol{M}$, respectively.

TABLE I. Summary of the symmetry of the torques observed in our experiments.

	IP FL, $\xi_{\text{FL},y}$	IP DL, $\xi_{\text{DL},y}$	OOP FL, $\xi_{\text{FL},z}$	OOP DL, $\xi_{\text{DL},z}$
Torque form	$\boldsymbol{y}\times\boldsymbol{M}$	$\boldsymbol{M}\times(\boldsymbol{M}\times\boldsymbol{y})$	$\boldsymbol{z}\times\boldsymbol{M}$	$\boldsymbol{M}\times(\boldsymbol{M}\times\boldsymbol{z})$
θ dependence in ST-FMR	$\sin2\theta\cos\theta$ in A	$\sin2\theta\cos\theta$ in S	$\sin2\theta$ in S	$\sin2\theta$ in A

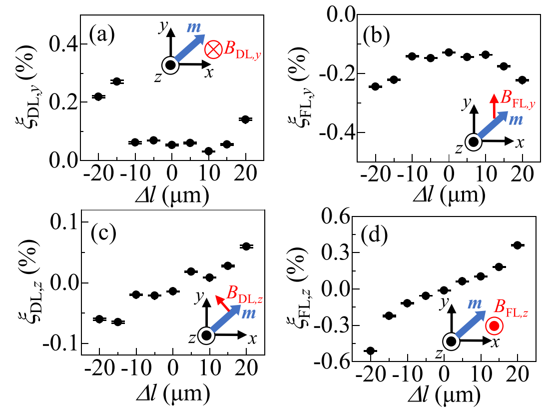

FIG. 3. Torque efficiencies as a function of Δl for (a) IP DL torque, $\xi_{\mathrm{DL},y}$; (b) IP FL torque, $\xi_{\mathrm{FL},y}$; (c) OOP DL torque, $\xi_{\mathrm{DL},z}$; and (d) OOP FL torque, $\xi_{\mathrm{FL},z}$. Insets show the directions of the effective magnetic fields that correspond to each torque when the electric current is along the x direction.

IV. TORQUE EFFICIENCIES AND ORIGINS OF OOP TORQUES

Figure 3(a)-3(d) shows each torque efficiency, ξ, as a function of Δl calculated by using relationships between ξ and B [15,16,26],

$$B_{\mathrm{DL(FL)}} = \xi_{\mathrm{DL(FL)}} \frac{\hbar I_{\mathrm{rf}}}{2eM_{\mathrm{S}}wt^2}, \tag{3}$$

and the insets show the directions of each effective magnetic field. Here, we determined I_{rf}, R_{AMR}, and M_{s} by additional experiments (Supplemental Material B [30,37]). Although we detected contributions of IP FL and DL torques as shown in Fig. 2, $\xi_{\mathrm{DL},y}$ and $\xi_{\mathrm{FL},y}$ are one or two orders of magnitude smaller than the typical values in the NM/FM bilayer structures. The enhancements of $\xi_{\mathrm{DL},y}$ and $\xi_{\mathrm{FL},y}$ at $\Delta l = \pm 20$ μm might be due to an increment of net spin current along the z direction via enhancement in asymmetry of the spin, magnetic, and structural properties along the z direction, induced by the large current density and/or Joule heating. The polarity of $\xi_{\mathrm{DL},y}$ and $\xi_{\mathrm{FL},y}$ is always positive and negative, respectively, and we confirmed no clear correlation with Δl, as shown in Figs. 3(a) and 3(b). In contrast, the OOP torques, $\xi_{\mathrm{DL},z}$ and $\xi_{\mathrm{FL},z}$, strongly depended on Δl. The positive correlation between the OOP torques and Δl indicates that the lateral inversion asymmetry was essential to generate the OOP torques. We note that enhancement of the IP torques at $\Delta l = \pm 20$ μm does not affect the estimation of the OOP torques because the OOP torques are separated from the IP torques using Eqs. (2a)–(2d).

Here, we discuss possible origins of the OOP FL and DL torques. The OOP FL torque can be simply understood as a consequence of the Ampere law. A finite magnetic field along the z direction because of Oersted field, B_{Oersted}, is expected because of the nonuniform charge current flow in the Py layer, resulting in an OOP FL torque [28,38]. In contrast, the mechanism of the OOP DL torque is unclear. We note that generation of the OOP DL torque is not restricted to a specific shape of the electrode shown in Fig. 1(a) and 1(b), because we obtained a finite OOP DL torque in devices with a different electrode structure, as discussed in Supplemental Material C [30]. One can imagine that the OOP spin accumulates at the edge of the Py layer because the SHE might contribute to the OOP DL torque. Because of the nonuniform flow of the electric current, the OOP spin at one side with a shorter length is more pertinent than that with a longer length. However, the sign of $\xi_{\mathrm{DL},z}$ via OOP spin accumulation at the edge should be opposite to the observed values considering the positive spin Hall angle of Py [39,40], indicating that the SHE is not a dominant contributor to the OOP DL torque. OOP spin polarization was recently reported when a spin along the magnetization direction was rotated by the Rashba effective field at the interface [41,42]. However, such torque has additional cosθ dependence, which is inconsistent with sin2θ behavior in A. In the same manner, the spin swap effect [43,44] and the magnetic SHE [6] are also excluded. The anomalous Nernst effect and the spin pumping are also not the dominant originators because they do not have sin2θ dependence (Tables S1 and S2 in Supplemental Material A) [26,30,33,45].

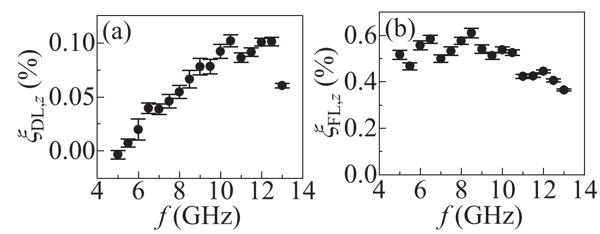

FIG. 4. Microwave frequency f dependence of (a) $\xi_{\mathrm{DL},z}$ and (b) $\xi_{\mathrm{FL},z}$ for $\Delta l = 20$ μm.

To reveal the origin of the OOP DL torque, we investigated the f dependence of ST-FMR signals. Figure 4(a) and 4(b) shows the f dependence of $\xi_{\mathrm{DL},z}$ and $\xi_{\mathrm{FL},z}$. Unexpectedly, $\xi_{\mathrm{DL},z}$ was considerably enhanced with increasing f, which differs from the conventional SOT originating from, for example, the SHE [25]. The aforementioned mechanisms are not a dominant factor because they are expected to have no f dependence. One plausible origin of the OOP DL torque is the inductive magnetic field. By applying B_{Oersted} via the nonuniform charge current, an inductive charge current (i.e., eddy current) is generated. Here, the phase of the eddy current is shifted by $\pi/2$ from B_{Oersted} because of Faraday's law. Finally, the eddy current generated an additional inductive magnetic field, $B_{\mathrm{induc.}}$, along the z direction, which is well known as the complex magnetic permeability [46]. This behavior becomes pronounced under the application of a magnetic field along the z direction, because a sufficient eddy current can be generated because of the large area of the Py film. The $B_{\mathrm{induc.}}$ acted as the OOP DL torque in the ST-FMR measurements because of the phase shift by $\pi/2$ (Supplemental Material D [30]). This hypothesis clearly explains the enhancement of $\xi_{\mathrm{DL},z}$ in the high f region [Fig. 4(a)] because the inductive effect was enhanced at high frequency. A slight reduction in $\xi_{\mathrm{FL},z}$ in the high f region [Fig. 4(b)] also can be explained in the framework of the inductive effect. When the inductive effect is dominant in $\xi_{\mathrm{FL},z}$, $\xi_{\mathrm{FL},z}$ (corresponding to the real part of the complex magnetic permeability) should decrease as $\xi_{\mathrm{DL},z}$ (corresponding to the imaginary part of the complex magnetic permeability) increases. The f dependences of $\xi_{\mathrm{FL},z}$ and $\xi_{\mathrm{DL},z}$ (Fig. 4) qualitatively correspond to those of the real and imaginary parts, respectively, of the complex magnetic permeability [46]. Therefore, we conclude that the resulting

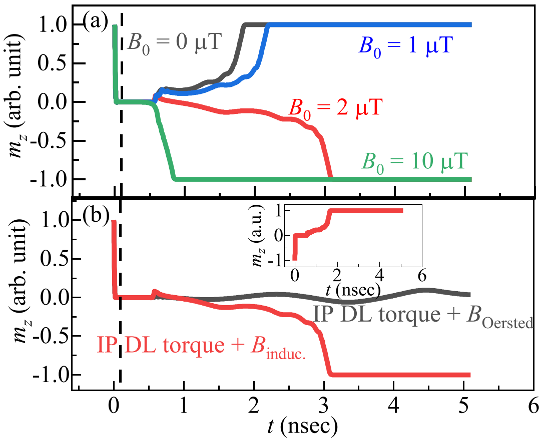

FIG. 5. Results of the time evolution of the z-component of magnetization, m_z, by a micromagnetic simulation. The simulation conditions correspond to the SOT magnetization switching of a FM/NM bilayer structure with asymmetric NM electrodes. We applied B_{Oersted} or $B_{\text{induc.}}$ along the OOP direction with or after application of the IP DL torque, respectively. Comparison of magnetization switching properties (a) under various amplitudes of $B_{\text{induc.}}$ and (b) under application of B_{Oersted} and $B_{\text{induc.}}$ with a magnitude of 2 μT. Result of $-z$ to $+z$ switching realized by inverting initial magnetization, injected spin orientation, and the sign of $B_{\text{induc.}}$ is also shown in the inset. We injected a 100-ps-width spin-polarized current at $t = 0$. We applied B_{Oersted} concomitantly with the spin-polarized current. We applied $B_{\text{induc.}}$ at $t = 100$ ps (indicated as a dotted line), which exponentially decayed. The spin current was injected from the bottom surface, which might cause a slight difference in the magnetization switching properties between $-z$ to $+z$ and $+z$ to $-z$.

OOP DL torque in this study is not due to the spin current along the z direction, but to the FL torque generated by the inductive field along the z direction.

V. EXTERNAL FIELD-FREE MAGNETIZATION SWITCHING USING $B_{\text{induc.}}$

We briefly comment on applications of $B_{\text{induc.}}$ with an asymmetric device structure in this study for SOT magnetization switching of PMA. Combining the IP torques and $B_{\text{induc.}}$ might enable fast and external field-free magnetization switching. If we use a heavy metal/PMA bilayer structure with asymmetric electrodes, the IP torques via the SHE of the heavy metal efficiently rotate magnetization. Within a short time after stopping the pulse current, during which only $B_{\text{induc.}}$ remains because of the inductive effect, magnetization is relaxed to the $-z$ direction by the perpendicular anisotropy field and $B_{\text{induc.}}$. To confirm the effect of $B_{\text{induc.}}$, we carried out a micromagnetic simulation using MuMax3 [47,48] (Supplemental Material E [30]). In the simulation, we used ferromagnetic materials with PMA. After we initialized magnetization along the $+z$ direction, we injected a spin current with $+y$ spins from the bottom plane. Subsequent to the spin-polarized current, we applied $B_{\text{induc.}}$ at $t = t_{\text{pls}} = 100$ ps. Here, $B_{\text{induc.}}$ decayed exponentially with a time constant $\tau = 500$ ps; i.e., $B_{\text{induc.}} = B_0 \exp[-(t-t_{\text{pls}})/\tau]$. Figure 5(a) shows the time evolution of the z component of the magnetization, m_z. We immediately aligned m_z along $+y$ by the IP DL torque. When $B_0 = 0$ and 1 μT, we did not achieve deterministic switching. However, when $B_0 > 2$ μT, m_z was successfully relaxed to the $-z$ direction, indicating SOT switching of PMA without an additional magnetic field. The magnitude of B_0 used in the simulation is comparable to that observed in our experiments, which is one-fifth of the typical value expected in the previous studies for the SOT switching of PMA; i.e., external field-free switching of PMA is possible by simply introducing asymmetry of the electrodes. We also realized magnetization reversal from $-z$ to $+z$ as shown in the inset of Fig. 5(b). Additionally, we realized switching of the PMA even when we changed temperature. We emphasize that B_{Oersted}, which we applied concomitantly with the spin-polarized current, cannot realize deterministic magnetization switching [Fig. 5(b)]. Therefore, a phase shift of the OOP magnetic field, $B_{\text{induc.}}$, is an important feature to induce external field-free magnetization switching.

Finally, we estimate the minimum device size to which the OOP inductive torque is applicable. Because $B_{\text{induc.}}$ originates from the eddy current, the minimum size that $B_{\text{induc.}}$ appears is scaled by the skin depth, δ (Supplemental Material F [30]) [49]. Here, δ is expressed as $\delta = 1/\sqrt{\pi f \mu_{\text{DC}} \mu_0 \sigma}$, where μ_{DC} is relative permeability in the DC limit, μ_0 is the magnetic permeability of free space, and σ is conductivity. Although the typical μ_{DC} of the ferromagnetic layer is $10^2 \sim 10^6$ [50], $\mu_{\text{DC}} = 1$ is suitable for estimation of δ because the magnetization immediately before generation of $B_{\text{induc.}}$ is kept along the in-plane direction due to the SOT, which substantially increases the minimum size for application of the OOP inductive torque. Using the typical value of σ, 1.0×10^6 Ω^{-1} m^{-1} of FM [51], and typical current density in PMA magnetization switching, 5×10^{11} A/m^2 [52], the minimum length of the rectangular PMA layer for generation of $B_{\text{induc.}} = 2$ μT is approximately 400 and 100 nm for the fall time of the pulse current of 100 and 10 ps, respectively. These values are rather large compared with those of a practical magnetic device. A pulse current with a steep change is desired to reduce the device size. However, we also propose a device structure for applying the OOP inductive torque to a much smaller device size. The proposed device has a NM/FM(PMA) or FM(PMA)/NM bilayer for generating SOT connected to asymmetric electrodes, and an isolated metal layer without any electric connection located beneath or on top of the PMA layer (Supplemental Material F [30]). In this case, the size of the metal layer can be designed freely and maximum $B_{\text{induc.}}$ can be realized by optimizing the size of the metal layer.

VI. CONCLUSION

We obtained additional components of current-induced torques, the symmetries of which with respect to the magnetic-field direction corresponded to the OOP DL and FL torques, in a single Py layer connected to electrodes with lateral asymmetry. We reversed the polarity of the torque by inverting the lateral symmetry of the electrodes. The OOP FL torque originated from the nonuniform charge current. In contrast, the OOP DL torque was not a real spin torque induced by spin-current injection but was due to the phase shift of the OOP FL torque generated by the inductive OOP magnetic field $B_{\text{induc.}}$. We proposed an alternative method for field-free

SOT magnetization switching of PMA by using $B_{\text{induc.}}$ instead of the real OOP DL torque generated by the spin current along the OOP direction. The micromagnetic simulation revealed the usefulness of $B_{\text{induc.}}$. Findings in this study provide a versatile method for the external field-free SOT switching of FM with PMA only by modulating the NM electrodes, and they contribute to further progress in MRAM technologies.

ACKNOWLEDGMENTS

This work was supported by Japan Society for the Promotion of Science (KAKENHI Grants No. 16H06330, No. 19H02197, No. 20H02607, and No. 20K22413), Japan Science and Technology Agency, and Precursory Research for Embryonic Science and Technology (Grant No. JPMJPR20B2).

[1] Y. K. Kato, Observation of the spin Hall effect in semiconductors, Science **306**, 1910 (2004).

[2] M. B. Lifshits and M. I. Dyakonov, Swapping Spin Currents: Interchanging Spin and Flow Directions, Phys. Rev. Lett. **103**, 186601 (2009).

[3] T. Taniguchi, J. Grollier, and M. D. Stiles, Spin-Transfer Torques Generated by the Anomalous Hall Effect and Anisotropic Magnetoresistance, Phys. Rev. Appl. **3**, 044001 (2015).

[4] D. Go, D. Jo, C. Kim, and H.-W. Lee, Intrinsic Spin and Orbital Hall Effects from Orbital Texture, Phys. Rev. Lett. **121**, 086602 (2018).

[5] G. Okano, M. Matsuo, Y. Ohnuma, S. Maekawa, and Y. Nozaki, Nonreciprocal Spin Current Generation in Surface-Oxidized Copper Films, Phys. Rev. Lett. **122**, 217701 (2019).

[6] A. Mook, R. R. Neumann, A. Johansson, J. Henk, and I. Mertig, Origin of the magnetic spin Hall Effect: Spin current vorticity in the Fermi sea, Phys. Rev. Research **2**, 023065 (2020).

[7] I. M. Miron, K. Garello, G. Gaudin, P. J. Zermatten, M. V. Costache, S. Auffret, S. Bandiera, B. Rodmacq, A. Schuhl, and P. Gambardella, Perpendicular switching of a single ferromagnetic layer induced by in-plane current injection, Nature (London) **476**, 189 (2011).

[8] L. Liu, C.- F. Pai, Y. Li, H. W. Tseng, D. C. Ralph, and R. A. Buhrman, Spin-torque switching with the giant spin Hall effect of tantalum, Science **336**, 555 (2012).

[9] M. DC, R. Grassi, J.-Y. Chen, M. Jamali, D. Reifsnyder Hickey, D. Zhang, Z. Zhao, H. Li, P. Quarterman, Y. Lv, M. Li, A. Manchon, K. A. Mkhoyan, T. Low, and J.-P. Wang, Room-temperature high spin-orbit torque due to quantum confinement in sputtered $Bi_xSe_{(1\text{-}x)}$ films, Nat. Mater. **17**, 800 (2018).

[10] Y.- T. Liu, T.- Y. Chen, T.- H. Lo, T.- Y. Tsai, S.- Y. Yang, Y.- J. Chang, J.- H. Wei, and C.- F. Pai, Determination of Spin-Orbit-Torque Efficiencies in Heterostructures with in-Plane Magnetic Anisotropy, Phys. Rev. Appl. **13**, 044032 (2020).

[11] M. Aoki, E. Shigematsu, M. Matsushima, R. Ohshima, S. Honda, T. Shinjo, M. Shiraishi, and Y. Ando, In-plane spin-orbit torque magnetization switching and its detection using the spin rectification effect at subgigahertz frequencies, Phys. Rev. B **102**, 174442 (2020).

[12] J. C. R. Sánchez, L. Vila, G. Desfonds, S. Gambarelli, J. P. Attané, J. M. De Teresa, C. Magén, and A. Fert, Spin-to-charge conversion using Rashba coupling at the interface between nonmagnetic materials, Nat. Commun. **4**, 2944 (2013).

[13] S. Emori, T. Nan, A. M. Belkessam, X. Wang, A. D. Matyushov, C. J. Babroski, Y. Gao, H. Lin, and N. X. Sun, Interfacial spin-orbit torque without bulk spin-orbit coupling, Phys. Rev. B **93**, 180402(R) (2016).

[14] V. P. Amin, J. Zemen, and M. D. Stiles, Interface-Generated Spin Currents, Phys. Rev. Lett. **121**, 136805 (2018).

[15] C.- F. Pai, Y. Ou, L. H. Vilela-Leão, D. C. Ralph, and R. A. Buhrman, Dependence of the efficiency of spin Hall torque on the transparency of Pt/ferromagnetic layer interfaces, Phys. Rev. B **92**, 064426 (2015).

[16] H. Hayashi, A. Musha, H. Sakimura, and K. Ando, Spin-orbit torques originating from the bulk and interface in Pt-based structures, Phys. Rev. Research **3**, 013042 (2021).

[17] C.- F. Pai, L. Liu, Y. Li, H. W. Tseng, D. C. Ralph, and R. A. Buhrman, Spin transfer torque devices utilizing the giant spin Hall effect of tungsten, Appl. Phys. Lett. **101**, 122404 (2012).

[18] M. Aoki, E. Shigematsu, R. Ohshima, T. Shinjo, M. Shiraishi, and Y. Ando, Coexistence of low-frequency spin-torque ferromagnetic resonance and unidirectional spin Hall magnetoresistance, Phys. Rev. B **104**, 094401 (2021).

[19] C. Zhang, Y. Takeuchi, S. Fukami, and H. Ohno, Field-free and sub-Ns magnetization switching of magnetic tunnel junctions by combining spin-transfer torque and spin–orbit torque, Appl. Phys. Lett. **118**, 092406 (2021).

[20] D. MacNeill, G. M. Stiehl, M. H. D. Guimaraes, R. A. Buhrman, J. Park, and D. C. Ralph, Control of spin–orbit torques through crystal symmetry in WTe_2/ferromagnet bilayers, Nat. Phys. **13**, 300 (2017).

[21] L. Liu, C. Zhou, X. Shu, C. Li, T. Zhao, W. Lin, J. Deng, Q. Xie, S. Chen, J. Zhou, R. Guo, H. Wang, J. Yu, S. Shi, P. Yang, S. Pennycook, A. Manchon, and J. Chen, Symmetry-dependent field-free switching of perpendicular magnetization, Nat. Nanotechnol. **16**, 277 (2021).

[22] A. Razavi, H. Wu, Q. Shao, C. Fang, B. Dai, K. Wong, X. Han, G. Yu, and K. L. Wang, Deterministic spin-orbit torque switching by a light-metal insertion, Nano Lett. **20**, 3703 (2020).

[23] Q. Ma, Y. Li, D. B. Gopman, Y. P. Kabanov, R. D. Shull, and C. L. Chien, Switching a Perpendicular Ferromagnetic Layer by Competing Spin Currents, Phys. Rev. Lett. **120**, 117703 (2018).

[24] Q. Shao, P. Li, L. Liu, H. Yang, S. Fukami, A. Razavi, H. Wu, K. Wang, F. Freimuth, Y. Mokrousov, M. D. Stiles, S. Emori, A. Hoffmann, J. Akerman, K. Roy, J.- P. Wang, S.- H. Yang, K. Garello, and W. Zhang, Roadmap of spin–orbit torques, IEEE Trans. Magn. **57**, 1 (2021).

[25] L. Liu, T. Moriyama, D. C. Ralph, and R. A. Buhrman, Spin-Torque Ferromagnetic Resonance Induced by the Spin Hall Effect, Phys. Rev. Lett. **106**, 036601 (2011).

[26] S. Karimeddiny, J. A. Mittelstaedt, R. A. Buhrman, and D. C. Ralph, Transverse and Longitudinal Spin-Torque

Ferromagnetic Resonance for Improved Measurement of Spin-Orbit Torque, Phys. Rev. Appl. **14**, 024024 (2020).

[27] C. Kittel, On the theory of ferromagnetic resonance absorption, Phys. Rev. **73**, 155 (1948).

[28] J. Sklenar, W. Zhang, M. B. Jungfleisch, H. Saglam, S. Grudichak, W. Jiang, J. E. Pearson, J. B. Ketterson, and A. Hoffmann, Unidirectional spin-torque driven magnetization dynamics, Phys. Rev. B **95**, 224431 (2017).

[29] T. Horaguchi, M. Matsuo, and Y. Nozaki, Highly accurate evaluation of spin-torque efficiency by measuring in-plane angular dependence of spin-torque ferromagnetic resonance, J. Magn. Magn. Mater. **505**, 166727 (2020).

[30] See Supplemental Material at http://link.aps.org/supplemental/10.1103/PhysRevB.105.144407 for more details on the angular dependence of the ST-FMR, parameters for estimation of the torque efficiencies, OOP torque via the inductive effect, micromagnetic simulation using MuMax3, observation of the OOP torques in devices with a different electrode structure, and proposal of the device structure for applying the OOP inductive torque.

[31] T. D. Skinner, K. Olejník, L. K. Cunningham, H. Kurebayashi, R. P. Campion, B. L. Gallagher, T. Jungwirth, and A. J. Ferguson, Complementary spin-Hall and Inverse spin-galvanic effect torques in a ferromagnet/semiconductor bilayer, Nat. Commun. **6**, 6730 (2015).

[32] J. Sklenar, W. Zhang, M. B. Jungfleisch, W. Jiang, H. Chang, J. E. Pearson, M. Wu, J. B. Ketterson, and A. Hoffmann, Driving and detecting ferromagnetic resonance in insulators with the spin Hall effect, Phys. Rev. B **92**, 174406 (2015).

[33] M. Harder, Y. Gui, and C.- M. Hu, Electrical detection of magnetization dynamics via spin rectification effects, Phys. Rep. **661**, 1 (2016).

[34] W. Wang, T. Wang, V. P. Amin, Y. Wang, A. Radhakrishnan, A. Davidson, S. R. Allen, T. J. Silva, H. Ohldag, D. Balzar, B. L. Zink, P. M. Haney, J. Q. Xiao, D. G. Cahill, V. O. Lorenz, and X. Fan, Anomalous spin–orbit torques in magnetic single-layer films, Nat. Nanotechnol. **14**, 819 (2019).

[35] T. Seki, Y.-C. Lau, S. Iihama, and K. Takanashi, Spin-orbit torque in a Ni-Fe single layer, Phys. Rev. B **104**, 094430 (2021).

[36] L. Zhu, D. C. Ralph, and R. A. Buhrman, Unveiling the mechanism of bulk spin-orbit torques within chemically disordered Fe_xPt_{1-x} single layers, Adv. Funct. Mater. **31**, 2103898 (2021).

[37] V. Tshitoyan, C. Ciccarelli, A. P. Mihai, M. Ali, A. C. Irvine, T. A. Moore, T. Jungwirth, and A. J. Ferguson, Electrical manipulation of ferromagnetic NiFe by antiferromagnetic IrMn, Phys. Rev. B **92**, 214406 (2015).

[38] T. Ikebuchi, T. Moriyama, Y. Shiota, and T. Ono, Homodyne detection of ferromagnetic resonance by a non-uniform radio-frequency excitation current, Appl. Phys. Express **11**, 053008 (2018).

[39] A. Tsukahara, Y. Ando, Y. Kitamura, H. Emoto, E. Shikoh, M. P. Delmo, T. Shinjo, and M. Shiraishi, Self-induced inverse spin Hall effect in permalloy at room temperature, Phys. Rev. B **89**, 235317 (2014).

[40] L. Leiva, S. Granville, Y. Zhang, S. Dushenko, E. Shigematsu, T. Shinjo, R. Ohshima, Y. Ando, and M. Shiraishi, Giant spin Hall angle in the Heusler alloy Weyl ferromagnet Co_2MnGa, Phys. Rev. B **103**, L041114 (2021).

[41] S. H. C. Baek, V. P. Amin, Y. W. Oh, G. Go, S. J. Lee, G. H. Lee, K. J. Kim, M. D. Stiles, B. G. Park, and K. J. Lee, Spin currents and spin-orbit torques in ferromagnetic trilayers, Nat. Mater. **17**, 509 (2018).

[42] Z. Luo, Q. Zhang, Y. Xu, Y. Yang, X. Zhang, and Y. Wu, Spin-Orbit Torque in a Single Ferromagnetic Layer Induced by Surface Spin Rotation, Phys. Rev. Appl. **11**, 064021 (2019).

[43] C. O. Pauyac, M. Chshiev, A. Manchon, and S. A. Nikolaev, Spin Hall and Spin Swapping Torques in Diffusive Ferromagnets, Phys. Rev. Lett. **120**, 176802 (2018).

[44] K.- W. Kim and K.- J. Lee, Generalized Spin Drift-Diffusion Formalism in the Presence of Spin-Orbit Interaction of Ferromagnets, Phys. Rev. Lett. **125**, 207205 (2020).

[45] A. Azevedo, R. O. Cunha, F. Estrada, O. Alves Santos, J. B. S. Mendes, L. H. Vilela-Leão, R. L. Rodríguez-Suárez, and S. M. Rezende, Electrical detection of ferromagnetic resonance in single layers of permalloy: Evidence of magnonic charge pumping, Phys. Rev. B **92**, 024402 (2015).

[46] R. B. Goldfarb and H. E. Bussey, Method for measuring complex permeability at radio frequencies, Rev. Sci. Instrum. **58**, 624 (1987).

[47] A. Vansteenkiste, J. Leliaert, M. Dvornik, M. Helsen, F. Garcia-Sanchez, and B. Van Waeyenberge, The design and verification of MuMax3, AIP Adv. **4**, 107133 (2014).

[48] J. Leliaert, J. Mulkers, J. De Clercq, A. Coene, M. Dvornik, and B. Van Waeyenberge, Adaptively time stepping the stochastic Landau-Lifshitz-Gilbert equation at nonzero temperature: Implementation and validation in MuMax 3, AIP Adv. **7**, 125010 (2017).

[49] J. E. L. Bishop and E. W. Lee, The behaviour of ferromagnetic sheets in alternating electric and magnetic fields II: Measurements of the electrical resistance of iron strips from 0 to 30 Mc/S, Proc. R. Soc. Lond. Ser. A. Math. Phys. Sci. **276**, 112 (1963).

[50] H. D. Arnold and G. W. Elmen, Permalloy, a new magnetic material of very high permeability, Bell Syst. Tech. J. **2**, 101 (1923).

[51] Q. Hao and G. Xiao, Giant Spin hall effect and magneto-transport in a Ta/CoFeB/MgO layered structure: A temperature dependence study, Phys. Rev. B **91**, 224413 (2015).

[52] L. Zhu, D. C. Ralph, and R. A. Buhrman, Lack of Simple Correlation Between Switching Current Density and Spin-Orbit-Torque Efficiency of Perpendicularly Magnetized Spin-Current-Generator–Ferromagnet Heterostructures, Phys. Rev. Appl. **15**, 024059 (2021).